

# Electronic Raman study of $\text{Ba}_{1-x}\text{K}_x\text{Fe}_2\text{As}_2$ from under-doping to over-doping

S.-F. Wu,<sup>1,2</sup> P. Richard,<sup>2,3,\*</sup> H. Ding,<sup>2,3</sup> H.-H. Wen,<sup>4,5</sup> Guotai Tan,<sup>6</sup>  
Meng Wang,<sup>7</sup> Chenglin Zhang,<sup>6</sup> Pengcheng Dai,<sup>6</sup> and G. Blumberg<sup>1,8,†</sup>

<sup>1</sup>*Department of Physics and Astronomy, Rutgers University, Piscataway, NJ 08854, USA*

<sup>2</sup>*Beijing National Laboratory for Condensed Matter Physics,  
and Institute of Physics, Chinese Academy of Sciences, Beijing 100190, China*

<sup>3</sup>*Collaborative Innovation Center of Quantum Matter, Beijing, China*

<sup>4</sup>*National Laboratory of Solid State Microstructures and Department of Physics, Nanjing University, Nanjing 210093, China*

<sup>5</sup>*Collaborative Innovation Center of Advanced Microstructures, Nanjing University, China*

<sup>6</sup>*Department of Physics and Astronomy, Rice University, Houston, TX 77005, USA*

<sup>7</sup>*Department of Physics, University of California, Berkeley, California 94720, USA*

<sup>8</sup>*National Institute of Chemical Physics and Biophysics, 12618 Tallinn, Estonia*

(Dated: August 23, 2016)

We performed an electronic Raman scattering study of under-doped, optimally-doped and over-doped  $\text{Ba}_{1-x}\text{K}_x\text{Fe}_2\text{As}_2$  samples, in the normal and superconducting states. We observe a quasi-elastic peak in the normal state in both the  $B_{1g}$  and  $B_{2g}$  channels for all the samples studied. We attribute this peak to nematic fluctuations. In the superconducting state, we observe two distinct superconducting pair breaking peaks corresponding to two superconducting gaps, a large one and a small one. In addition, we detect a collective mode below the superconducting transition in the  $B_{2g}$  channel and we determine its doping evolution. Although the energy of the mode is consistent with that of the neutron resonance mode, its nature remains unclear as Raman scattering probes singlet excitations at zero momentum transfer whereas the neutron resonance mode occurs in the triplet channel at a fixed wave vector. Different scenarios are proposed to explain the Raman collective mode. In the superconducting state of the under-doped regime, we find a transition or crossover temperature below which the spectral background changes and the collective mode vanishes, thus imposing constraints on the possible candidates to explain its origin.

PACS numbers: 74.70.Xa, 74.25.nd

## I. INTRODUCTION

Multi-band systems often exhibit complex phase diagrams shaped by low-energy many-body interactions. Host to spin-density-waves, nematicity and superconductivity, the Fe-based superconductors provide a suitable playground for studying low-energy many-body interactions and collective modes. Although still debated, many theories claim that the unconventional superconductivity of the Fe-based superconductors itself derives from low-energy electronic interactions [1, 2] (see Ref. [3] for a recent review), thus justifying the quest for a thorough understanding of their nature.

One of the hallmarks of unconventional superconductivity and of the main signatures of collective excitations in the cuprates is a neutron spin resonance mode appearing below the superconducting critical temperature ( $T_c$ ) at the antiferromagnetic wave vector  $\mathbf{Q}$  [4–10]. Despite extensive research activities, its interplay with superconductivity remains unclear. Interestingly, such a mode has also been detected at 14 meV in the archetype Fe-based superconductor  $\text{Ba}_{0.6}\text{K}_{0.4}\text{Fe}_2\text{As}_2$  [11, 12], with corresponding signatures in angle-resolved photoemission spectroscopy (ARPES) [13] and scanning tunneling spectroscopy (STS) [14]. These experimental observations

confirm the existence of collective excitations in the Fe-based superconductors. However, due to the complex coupling between the spin and orbital degrees of freedom [15], there is still no consensus on their precise nature.

Recent electronic Raman spectroscopy studies reveal a sharp mode at  $140 \text{ cm}^{-1}$  (17.5 meV) in optimally-doped  $\text{Ba}_{0.6}\text{K}_{0.4}\text{Fe}_2\text{As}_2$  [16–18] in the  $B_{2g}$  channel. The mode was interpreted in terms of a Bardasis-Schrieffer (BS) mode in the particle-particle channel [19–22], as a result of the attractive residual interactions in the sub-leading  $d$ -wave pairing channel [23, 24]. This interpretation differs from that of Gallais *et al.*, who claim that a similar mode in Co-doped  $\text{BaFe}_2\text{As}_2$  originates from nematic fluctuations in the presence of the superconducting (SC) gap [25]. Two collective modes were also reported in the  $B_{2g}$  symmetry channel of  $\text{NaFe}_{1-x}\text{Co}_x\text{As}$  and assigned by Thorsmølle *et al.* [26] to a particle-hole exciton due to the attractive  $d$ -wave density-density interaction [27, 28] and to a particle-particle BS mode. Obviously, the origin of the interactions leading to these in-gap collective modes remains unresolved and calls for more extensive studies.

Here we present a Raman scattering study of under-doped, optimally-doped and over-doped  $\text{Ba}_{1-x}\text{K}_x\text{Fe}_2\text{As}_2$  samples. In the normal state, we observe quasi-elastic scattering in both the  $B_{1g}$  and  $B_{2g}$  channels that we attribute to nematic fluctuations. In the SC state, we detect two coherence SC pair breaking peaks corresponding to a large and a small SC gaps. The energies of these

\* p.richard@iphy.ac.cn

† girsh@physics.rutgers.edu

peaks are consistent with results obtained with different spectroscopic techniques. In addition, we observe a sharp in-gap collective mode in the  $B_{2g}$  channel at an energy that is similar to that of the neutron resonance mode. Although the origin of this mode remains unclear due to the difference in the momentum transfer associated to the Raman and neutron modes, we discuss a few potential candidates. Interestingly, we detect a transition or crossover temperature in the under-doped regime below which the electronic spectral background changes and the collective mode disappears, thus signifying a phase transition inside the SC dome and putting constraints on the origin of this Raman mode.

## II. EXPERIMENT

Single crystals of  $Ba_{1-x}K_xFe_2As_2$  ( $x = 0.25, 0.4$  and  $0.6$ , with  $T_c$  values of 31 K, 38 K and 25 K, respectively) were grown by the self-flux method as described in Ref. [29]. In the text, these samples are labeled UD (under-doped), OPD (optimally-doped) and OD (over-doped), respectively. The crystals used for Raman scattering were cleaved in nitrogen gas atmosphere and positioned in a continuous flow liquid Helium optical cryostat. Since the optimally-doped sample was cleaved twice, the corresponding sets of data are labeled “OPD#1” and “OPD#2”. The measurements presented here were performed in a quasi-back scattering geometry along the  $c$ -axis using a  $Kr^+$  ion laser. Except for the inset of Fig. 5(c), for which the 752 nm (1.65 eV) laser line was used, all data were recorded with the line at 647.1 nm (1.92 eV) excitation. The incident laser beam was focused onto a  $50 \times 100 \mu m^2$  spot on the  $ab$ -surface, with an incident power smaller than 10 and 3 mW for measurements in the normal and SC states, respectively. The scattered light was collected and analyzed by a triple-stage Raman spectrometer designed for high-stray light rejection and throughput, and recorded using a liquid nitrogen-cooled charge-coupled detector. The Raman spectra were corrected for the spectral responses of the spectrometer and detector. The temperature has been corrected for laser heating.

In this manuscript, we define X and Y along the 2 Fe unit cell crystallographic axes  $a$  and  $b$  (at  $45^\circ$  degrees from the Fe-Fe direction) in the tetragonal phase, whereas X' and Y' are along the Fe-Fe directions, as shown in Figs. 1(a)-1(b).

For crystals with the  $D_{4h}$  point group symmetry, the XX, X'Y' and XY Raman geometries probe the  $A_{1g}+B_{1g}$ ,  $A_{2g}+B_{1g}$  and  $A_{2g}+B_{2g}$  channels, respectively [30]. Assuming the same featureless luminescence background  $I_{BG}$  for all symmetry channels and that the  $A_{2g}$  response is negligible, the imaginary part of the Raman susceptibility in the  $A_{1g}$  channel can be obtained by subtracting the X'Y' spectrum from the XX spectrum, and then by dividing the result by the Bose-Einstein factor  $1+n(\omega, T)$ . The imaginary part of Raman susceptibility

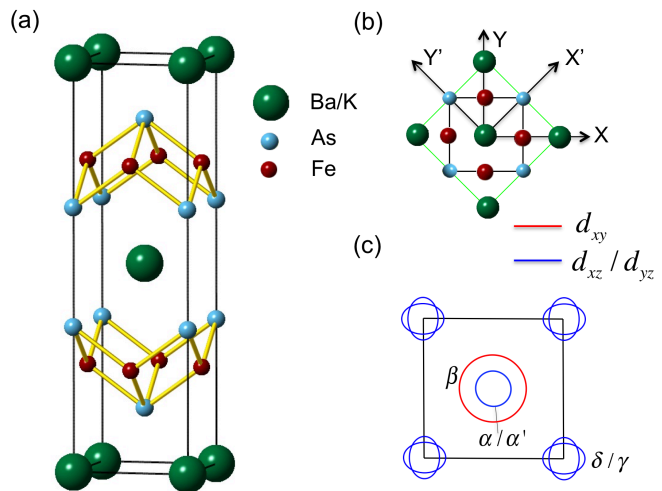


FIG. 1. (Color online) (a) Crystal structure of  $Ba_{1-x}K_xFe_2As_2$ . (b) Definition of the X, Y, X' and Y' directions. The green and black lines represent the 4-Fe and 2-Fe unit cells, respectively. (c) Schematic representation of the Fermi surface of  $Ba_{1-x}K_xFe_2As_2$  in the 2-Fe Brillouin zone.

in the  $B_{1g}$  and  $B_{2g}$  channels can be easily obtained from X'Y' and XY spectra, respectively.

## III. RESULTS

### A. Normal state

In Figs. 2(a)-2(i), we show the normal state Raman spectra of  $Ba_{1-x}K_xFe_2As_2$  in three different channels. The sharp peak around  $182 \text{ cm}^{-1}$  detected at room temperature in Figs. 2(a)-2(c) corresponds to a  $A_{1g}$  phonon. This mode shifts to high energy upon cooling [31] and its intensity becomes stronger as K doping increases. In the  $B_{2g}$  channel [Figs. 2(d)-2(f)], the electronic continuum gets enhanced from 300 K to 40 K. In particular, a low-energy peak similar to one previously assigned to a  $B_{2g}$  type of nematic fluctuations develops at low temperature around  $100 \text{ cm}^{-1}$  [26, 32]. We note that the normal state intensity of this quasi-elastic peak in  $Ba_{1-x}K_xFe_2As_2$  is much weaker than in  $Ba(Fe_{1-x}Co_x)_2As_2$  [33–35], which is possibly due to the different anisotropic properties of the electron-doped and hole-doped Fe-based superconductors reported also by resistivity measurements [36, 37]. Except for the sharp  $B_{1g}$  phonon peak at  $208 \text{ cm}^{-1}$  at room temperature, we also detect a similar quasi-elastic scattering in the  $B_{1g}$  channel [Figs. 2(g)-2(i)], suggesting the existence of  $B_{1g}$  type charge fluctuations [38]. Though weaker, the  $B_{1g}$  quasi-elastic peak intensity builds up upon cooling. The quasi-elastic scattering has comparable strength in the  $B_{1g}$  and  $B_{2g}$  channels at optimal doping.

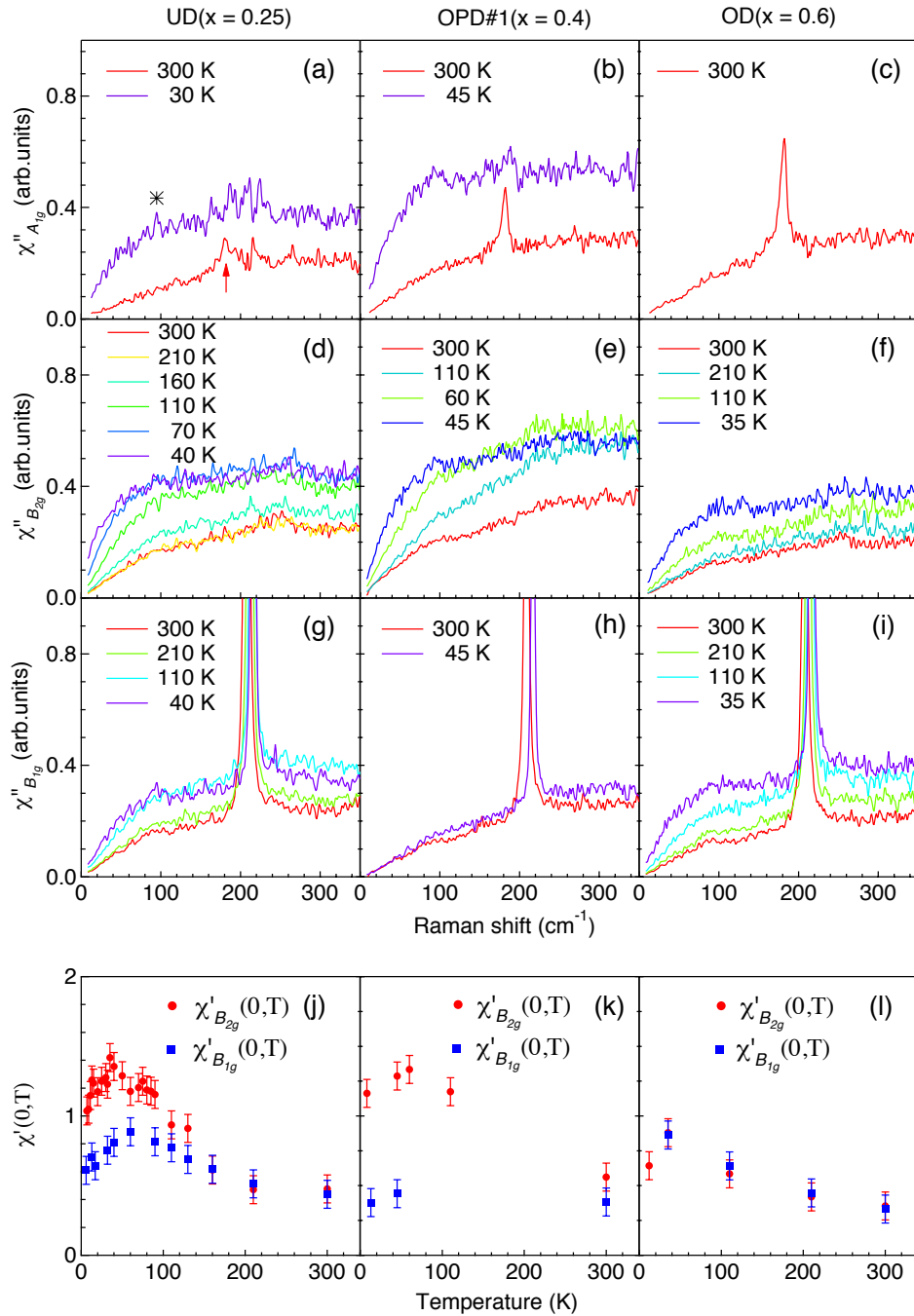


FIG. 2. (Color online). Doping and temperature evolution of the Raman susceptibility of Ba<sub>1-x</sub>K<sub>x</sub>Fe<sub>2</sub>As<sub>2</sub> in different symmetry channels. Left column: UD ( $x = 0.25$ ); Central column: OPD#1 ( $x = 0.4$ ); Right column: OD ( $x = 0.6$ ). (a)-(c) Temperature dependence of the Raman response in the A<sub>1g</sub> channel. The asterisk in (a) marks a small peak due to laser plasma, whereas the arrow indicates a A<sub>1g</sub> phonon. (d)-(f) Temperature dependence of the Raman response in the B<sub>2g</sub> channel. (g)-(i) Same as (d)-(f) but for the B<sub>1g</sub> channel. (j)-(l)  $T$ -dependence of the static Raman susceptibilities  $\chi'_{B_{2g}}(0,T)$  (red solid circles) and  $\chi'_{B_{1g}}(0,T)$  (blue solid squares).

In Figs. 2(j)-2(l), we show the static Raman susceptibilities  $\chi'_{B_{1g}}(0,T)$  and  $\chi'_{B_{2g}}(0,T)$  obtained *via* the Kramers-Kronig transformation with a high-energy cut-off at 350 cm<sup>-1</sup> justified by an already small  $\chi''(\omega)/\omega$

integrand of the Kramers-Kronig transformation at that energy. We used a linear function to extrapolate the  $\chi''(\omega)$  function to zero in both B<sub>1g</sub> and B<sub>2g</sub> channels. The B<sub>1g</sub> phonon was removed by fitting before the Kramers-

TABLE I. Summary of the SC gaps and bosonic modes deduced from Raman scattering, ARPES, STS and inelastic neutron scattering (INS). Energies are given in meV. UD, OPD and OD refer to under-doped, optimally-doped and over-doped samples, respectively. We caution that the doping of the under-doped and over-doped samples measured by different techniques may be different and that the collective modes observed in Raman and in the other types of spectroscopies may have different origins.

|                         | Raman<br>(This work) | Raman<br>([16, 17]) | ARPES        | STS       | INS       |
|-------------------------|----------------------|---------------------|--------------|-----------|-----------|
| $\Delta_\alpha^{(UD)}$  |                      |                     | 9 [39]       | 6 [40]    |           |
| $\Delta_\beta^{(UD)}$   | 3.8                  |                     | 4 [39]       | 3.8 [40]  |           |
| $E_{CM}^{(UD)}$         | 12                   |                     |              | 8 [40]    | 12.5 [41] |
| $\Delta_\alpha^{(OPD)}$ | 10.8 ( $B_{2g}$ )    | 10.6                | 9-13 [42-44] | 10.5 [45] |           |
| $\Delta_\beta^{(OPD)}$  | 4.4                  | 4.4                 | 5-6 [42-44]  | 6 [45]    |           |
| $E_{CM}^{(OPD)}$        | 17.5                 | 17.5                | 13±2 [13]    | 14 [14]   | 14 [11]   |
| $\Delta_\alpha^{(OD)}$  | 10                   |                     | 8 [46]       | 6 [45]    |           |
| $\Delta_\beta^{(OD)}$   | 3                    |                     | 4 [46]       | 3 [45]    |           |
| $E_{CM}^{(OD)}$         | 14                   |                     |              |           | 12 [47]   |

Kronig transformation. Both static Raman susceptibilities  $\chi'_{B_{1g}}(0, T)$  and  $\chi'_{B_{2g}}(0, T)$  get enhanced upon cooling. In Fig. 2(j),  $\chi'_{B_{1g}}(0, T)$  shows a broad peak with a maximum around 60 K, whereas  $\chi'_{B_{2g}}(0, T)$  shows a maximum around  $T_c$ . The static Raman susceptibility  $\chi'_{B_{2g}}(0, T)$  is significantly larger than  $\chi'_{B_{1g}}(0, T)$  in the under-doped [Fig. 2 (k)] and optimally-doped [Fig. 2 (l)] samples, suggesting that the  $B_{2g}$  channel is the dominant channel for the charge quadrupole fluctuations at low doping. However, both susceptibilities have similar intensities in the over-doped regime. In a recent study of  $\text{BaFe}_2(\text{As}_{0.5}\text{P}_{0.5})_2$ , it was argued that the similarity between the  $\chi'_{B_{1g}}(0, T)$  and  $\chi'_{B_{2g}}(0, T)$  static susceptibilities could originate from the local breakdown of the  $\sigma_d$  and  $\sigma_v$  symmetry planes due to (As,P) disorder [38]. The same argument could also apply here due to the (Ba,K) disorder.

## B. Superconducting state

Before discussing the Raman scattering features observed at low temperature, it is good to recall the SC gap values obtained by other spectroscopic probes in optimally-doped  $\text{Ba}_{1-x}\text{K}_x\text{Fe}_2\text{As}_2$ . ARPES studies report nodeless SC gaps on all Fermi surface (FS) pockets, with small or negligible in-plane anisotropy [42, 43]. While a SC gap of 6 meV is found on the holelike  $\beta$  ( $d_{xy}$ ) FS centered at the  $\Gamma$  point, a larger gap of about 12 meV is found on all the other pockets, with only small differences (about 1 meV) from one FS pocket to the other [44]. An ARPES study of the SC gap using synchrotron radiation, which allows to vary the  $k_z$  position, indicates

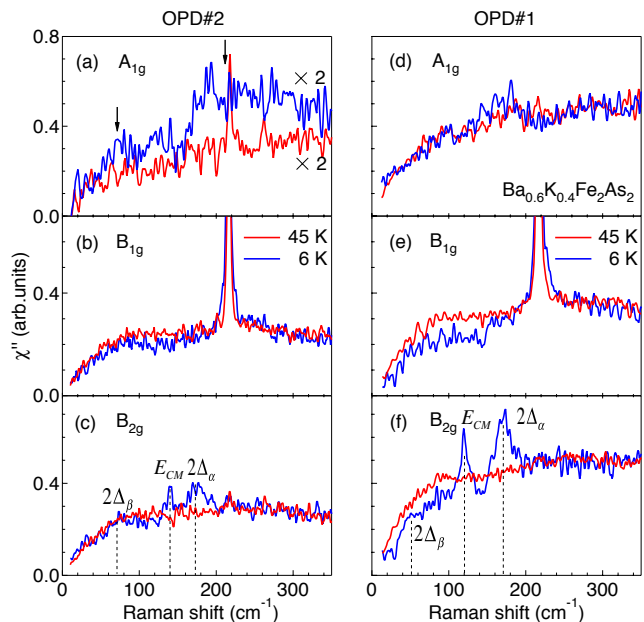


FIG. 3. (Color online) (a)-(c) Raman response of  $\text{Ba}_{0.4}\text{K}_{0.6}\text{Fe}_2\text{As}_2$  (OPD#2) at 45 K (red) and 6 K (blue) in the (a)  $A_{1g}$ , (b)  $B_{1g}$ , and (c)  $B_{2g}$  channels. The dashed lines in (c) mark a broad feature at  $70 \text{ cm}^{-1}$  ( $2\Delta_\beta$ ), a collective mode ( $E_{CM}$ ) around  $140 \text{ cm}^{-1}$  and a pair-breaking peak at  $172 \text{ cm}^{-1}$  ( $2\Delta_\alpha$ ). (d)-(f) Same as (a)-(c) but for sample OPD#1. For the OPD#1 sample we find  $2\Delta_\beta = 50 \text{ cm}^{-1}$ ,  $E_{CM} = 120 \text{ cm}^{-1}$  and  $2\Delta_\alpha = 168 \text{ cm}^{-1}$ .

that the gap size on each FS does not vary significantly with  $k_z$ , except for the  $\Gamma$ -centered hole FS formed by the even combination of the  $d_{xz}$  and  $d_{yz}$  orbitals, for which a gap varying between 9 and 12 meV is recorded [48]. Results compatible with ARPES are obtained by STS, which reveals two coherence SC peaks at 10.5 meV and 6 meV [45], and by optical conductivity, for which a SC gap of 12.5 meV opens below  $T_c$  [49]. Although they do not provide a SC gap size, thermal conductivity measurements confirm the nodeless nature of the optimally-doped compound [50]. At the energy scale as the SC gaps, a 14 meV neutron resonance mode is reported below  $T_c$  at the antiferromagnetic wave-vector  $\mathbf{Q}$  [11]. Interestingly, a  $13 \pm 2$  meV mode energy determined from a kink in the electronic dispersion is observed by ARPES below  $T_c$  on bands quasi-nested by the antiferromagnetic wave-vector, indicating that the two modes have the same origin [13]. STS measurements also reveal a bosonic mode at 14 meV [14]. We summarize values of the SC gaps and bosonic modes deduced from different spectroscopies in TABLE I.

### 1. Optimal doping

In Fig. 3, we compare the Raman spectra at 45 K (normal state) and 6 K (SC state) in three symmetry channels

from optimally-doped samples OPD#1 and OPD#2. We first start describing results from the OPD#2 sample. In Fig. 3(a), two broad and weak features seem to emerge around  $70\text{ cm}^{-1}$  and  $210\text{ cm}^{-1}$ , which we assign to  $A_{1g}$  SC pair breaking peaks corresponding with single gap values  $\Delta$  of 4.4 meV and 13.1 meV, respectively. In Fig. 3(b), a small spectral weight suppression is seen below  $160\text{ cm}^{-1}$  in the  $B_{1g}$  channel. In Fig. 3(c), a broad and weak feature at  $70\text{ cm}^{-1}$  (8.8 meV) is observed in the  $B_{2g}$  channel, which we assign to the small gap  $2\Delta_\beta$  on the  $\beta$  FS pocket with  $d_{xy}$  character [42, 43]. Another sharp mode at  $172\text{ cm}^{-1}$  associated with a SC pair breaking peak at  $\Delta_\alpha = 10.8\text{ meV}$  appears in the  $B_{2g}$  channel, which is consistent with the 10-13 meV magnitude measured by ARPES for the large SC gap around  $k_z = 0$  [42–44]. The large gap value varies from 10.8 meV in the  $B_{2g}$  channel to 13.1 in the  $A_{1g}$  channel, suggesting an anisotropy, in agreement with ARPES measurements revealing an anisotropic gap along  $k_z$  [48]. Between the broad feature at  $70\text{ cm}^{-1}$  and the sharp peak at  $172\text{ cm}^{-1}$ , we detect a sharp mode at  $E_{CM} = 140\text{ cm}^{-1}$  (17.5 meV), which will be discussed further below.

As compared with the OPD#2 sample, the  $A_{1g}$  Raman response of the OPD#1 sample, shown in Fig. 3(d), becomes weaker and only a small broad peak is seen around  $160\text{ cm}^{-1}$ . In contrast, the spectral features in the  $B_{1g}$  and  $B_{2g}$  channels appear more clearly for the OPD#1 sample than for the OPD#2 sample. In Fig. 3(e), a clear spectral weight suppression below  $T_c$  is seen below  $160\text{ cm}^{-1}$  in the  $B_{1g}$  channel. In the  $B_{2g}$  channel, two sharp modes at  $120\text{ cm}^{-1}$  and  $168\text{ cm}^{-1}$ , as well as a kink feature at  $50\text{ cm}^{-1}$ , are seen in Fig. 3(f). While little change is observed for the large SC gap pair breaking peak as compared with the OPD#2 sample, a substantial shift from  $70\text{ cm}^{-1}$  to  $50\text{ cm}^{-1}$  is observed for the small SC gap pair breaking peak. The sharp  $E_{CM}$  mode shifts by the same amount, from  $140\text{ cm}^{-1}$  to  $120\text{ cm}^{-1}$  in the OPD#1 sample. Since our Raman results on the OPD#2 sample are consistent with a previous Raman work [16] on the optimally-doped compound, we caution that our OPD#1 sample is possibly not optimally-doped. It could have a slightly different doping due to inhomogeneous K distribution in the bulk or rapid sample aging.

In addition to the sharp peak, a threshold is also observed around  $30\text{ cm}^{-1}$  in the SC state [Figs. 3(e) and 3(f)]. This threshold suggests a fundamental gap of 1.9 meV below which the density-of-states vanishes, which is consistent with the 2 meV-wide flat bottom in the STS spectra [45]. The threshold is an evidence of fully-gapped superconductivity. No clear threshold is detected in the OPD#2 sample though, possibly because the cleaved surface is not good enough, as suggested by weaker peaks in the  $B_{2g}$  channel.

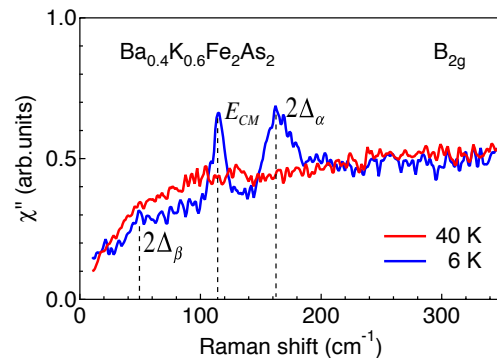


FIG. 4. (Color online) Raman response of  $\text{Ba}_{0.6}\text{K}_{0.4}\text{Fe}_2\text{As}_2$  (OD) at 40 K (red) and 6 K (blue) in the  $B_{2g}$  channel. The dashed lines mark a broad peak at  $50\text{ cm}^{-1}$  ( $2\Delta_\beta$ ), a collective mode  $E_{CM}$  at  $115\text{ cm}^{-1}$  and a pair breaking peak at  $162\text{ cm}^{-1}$  ( $2\Delta_\alpha$ ).

## 2. Over-doped regime

In the previous section we demonstrated that the spectral features observed in the Raman spectra of optimally-doped samples are consistent with data obtained from different spectroscopic probes. We now switch to the over-doped sample. In Fig. 4, we compare the Raman response obtained for the OD sample at 40 K (normal state) and 6 K (SC state) in the  $B_{2g}$  channel. Four features are clearly observed: a threshold around  $30\text{ cm}^{-1}$ , a kink-like feature around  $50\text{ cm}^{-1}$ , and two sharp modes at  $115\text{ cm}^{-1}$  and  $162\text{ cm}^{-1}$ . As with the OPD#1 sample, the threshold is assigned to a fundamental SC gap. The kink around  $50\text{ cm}^{-1}$  corresponds to the small SC gap pair breaking peak with  $\Delta_\beta = 3\text{ meV}$ . The sharp mode at  $162\text{ cm}^{-1}$  corresponds to the large SC gap pair breaking peak with  $\Delta_\alpha = 10\text{ meV}$ . As a comparison, an ARPES study on over-doped  $\text{Ba}_{0.7}\text{K}_{0.3}\text{Fe}_2\text{As}_2$  ( $T_c = 22\text{ K}$ ) gives  $\Delta_\alpha = 8\text{ meV}$  and  $\Delta_\beta = 4\text{ meV}$  [46]. Finally, the sharp mode at  $115\text{ cm}^{-1}$  (14 meV) is associated to the  $E_{CM}$  mode. We note that the Raman peak values from the OD sample are very close to those obtained on the OPD#1 sample, confirming that the OPD#1 sample might be slightly over-doped.

## 3. Under-doped regime

We now use the sensitivity of Raman scattering to obtain additional information in the under-doped regime. In the left column of Fig. 5, we compare the Raman responses  $\chi''(\omega)$  from the under-doped sample at 40 K (normal state) and 6 K (SC state) in three symmetry channels. A small suppression of spectral weight is observed below  $T_c$  at low energies in the  $A_{1g}$  channel [Fig. 5(a)], and the spectra barely change in the  $B_{1g}$  channel [Fig. 5(b)]. In the  $B_{2g}$  channel, however, spectral weight is transferred from the low-energy continuum and

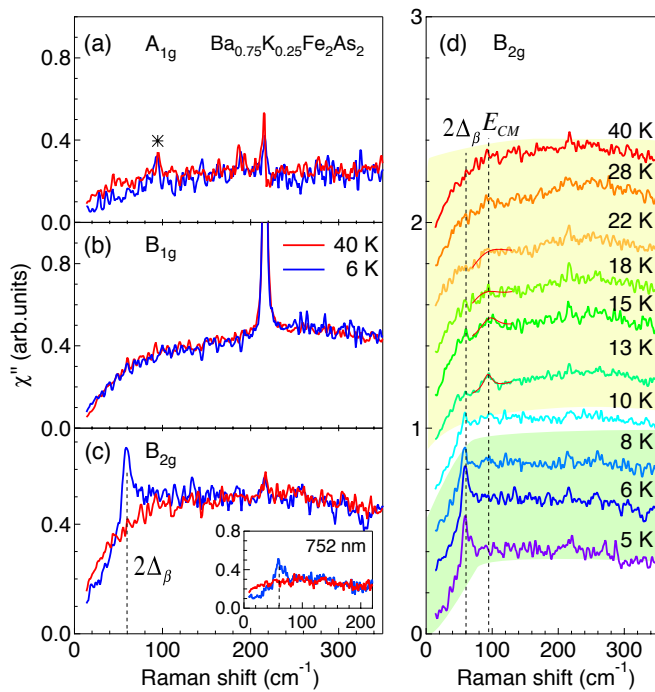


FIG. 5. (Color online). Raman response of  $\text{Ba}_{0.75}\text{K}_{0.25}\text{Fe}_2\text{As}_2$  (UD30K) at 40 K (red) and 6 K (blue) for the (a)  $A_{1g}$ , (b)  $B_{1g}$ , and (c)  $B_{2g}$  symmetries. The star in (a) represents a laser plasma line. The inset in (c) shows the Raman responses recorded with a 752 nm laser excitation. (d)  $\chi''_{B_{2g}}(\omega)$  at various temperatures. The dashed lines in (d) indicate  $2\Delta_\beta$  and  $E_{CM}$ . The red curves in (d) are fits of the  $E_{CM}$  peaks. The yellow and green shadings emphasize different spectral backgrounds associated to different phases.

builds up a sharp peak at  $60\text{ cm}^{-1}$  that contrasts with the weak kink observed at  $70\text{ cm}^{-1}$  in the optimally-doped samples. This peak is also seen when using a 752 nm laser excitation, as shown in the inset of Fig. 5(c). Following our interpretation of the kink observed at  $70\text{ cm}^{-1}$  at optimal doping, we attribute the  $60\text{ cm}^{-1}$  feature in the UD sample to a pair breaking peak with  $\Delta_\beta = 3.8\text{ meV}$ , which is consistent with the 4 meV gap value reported by ARPES measurements on the  $\beta$  ( $d_{xy}$ )  $\Gamma$ -centered hole FS pocket for samples with similar doping level [39]. Surprisingly, the sharp SC pair breaking peak at  $172\text{ cm}^{-1}$  observed at low temperature in the  $B_{2g}$  channel of our optimally-doped samples is absent in the UD sample. Although the reason for this behavior is unclear, we caution that it may be related to the loss of coherence also observed by ARPES experiments on the  $d_{xz}/d_{yz}$  bands of under-doped samples [39].

As illustrated by the fine temperature dependence of the  $B_{2g}$  Raman response in Fig. 5(d), the sharp peak at  $60\text{ cm}^{-1}$  appears clearly only at 10 K and below. Interestingly, the  $B_{2g}$  spectrum exhibits clear changes across that temperature, as highlighted with yellow and green backgrounds in Fig. 5(d). For example, the spectral background is flat below 10 K between  $100\text{ cm}^{-1}$  and

$350\text{ cm}^{-1}$ , but shows a broad feature above that temperature. These observations are consistent with recent studies on  $\text{Ba}_{1-x}\text{K}_x\text{Fe}_2\text{As}_2$  [51, 52] and  $\text{Ba}_{1-x}\text{Na}_x\text{Fe}_2\text{As}_2$  [53, 54] suggesting a complicated phase diagram in the under-doped regime. Within this context, the broad feature above 10 K can be interpreted as the formation of a spin-density-wave gap below the magnetic phase transition. We note that a pseudo-gap of about 17 meV was observed by ARPES below 125 K in under-doped  $\text{Ba}_{0.75}\text{K}_{0.25}\text{Fe}_2\text{As}_2$  [39]. Assuming that this pseudo-gap is approximately symmetric with respect to the Fermi energy, this would lead to a Raman feature at twice this value ( $274\text{ cm}^{-1}$ ), which is roughly the position of the broad feature observed here in our Raman data. The sudden disappearance of the broad feature below 10 K could be explained either by a non-magnetic low-temperature phase ( $T < 10\text{ K}$ ), which would contradict the phase diagram presented in Ref. [51], by a different magnetic structure that couples differently with light, or by broken four-fold symmetry at the lowest temperature. The  $E_{CM}$  mode in the UD sample is detected around  $95\text{ cm}^{-1}$  only between 22 K to 13 K, emphasizing further the contrast between the phases above and below the phase transition or crossover at 10 K. The disappearance of the  $E_{CM}$  mode below 10 K suggests a possible relationship with the magnetic structure or broken  $C_4$  symmetry.

#### IV. DISCUSSION

In this section we discuss possible explanations for the origin of the  $E_{CM}$  mode. In Fig. 6(b), we show, for various dopings, the difference between the Raman  $B_{2g}$  spectra recorded at 6 K and in the normal state. Although both the  $2\Delta_\alpha$  and  $2\Delta_\beta$  peaks shift with doping, the shift is significantly more pronounced for the later one [see Fig. 6(c)]. Interestingly, the  $E_{CM}$  mode moves almost by the same amount as the  $2\Delta_\beta$  peak. It is observed at  $95\text{ cm}^{-1}$  (11.9 meV) in  $\text{Ba}_{0.75}\text{K}_{0.25}\text{Fe}_2\text{As}_2$ ,  $140\text{ cm}^{-1}$  (17.5 meV) in  $\text{Ba}_{0.6}\text{K}_{0.4}\text{Fe}_2\text{As}_2$  and  $115\text{ cm}^{-1}$  (14.4 meV) in  $\text{Ba}_{0.4}\text{K}_{0.6}\text{Fe}_2\text{As}_2$ . If we assumed that it is a SC pair breaking peak, the mode at  $140\text{ cm}^{-1}$  at optimal doping would lead to  $\Delta = 8.8\text{ meV}$ , which is higher than the 6 meV SC gap typically observed by ARPES for the  $\beta$  ( $d_{xy}$ ) band and much smaller than the 11-13 meV gap observed on the other FSs [42, 43]. Similarly, in the UD sample the  $95\text{ cm}^{-1}$  energy of the mode would lead to  $\Delta = 6\text{ meV}$ , which is higher than the 4 meV SC gap observed by ARPES for the  $\beta$  ( $d_{xy}$ ) band, and much smaller than the 9-10 meV gap recorded on the other FSs [39]. Consequently, the  $E_{CM}$  peak is unlikely related to a SC pair breaking peak.

Interestingly, the energy scale of the  $E_{CM}$  mode is similar to that of the neutron resonance mode observed only below  $T_c$  in the triplet channel at the antiferromagnetic wave vector [11] and to the ARPES kink observed also only below  $T_c$ , practically with the same energy, on FSs quasi-nested by the same antiferromagnetic wave vec-

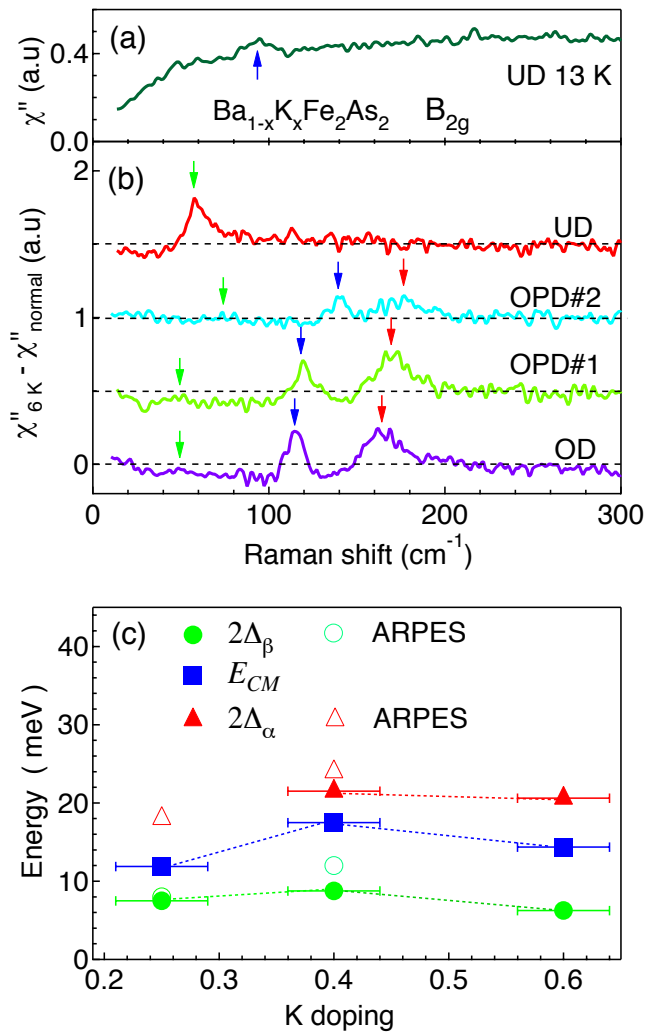


FIG. 6. (Color online). (a) Raman response of Ba<sub>0.75</sub>K<sub>0.25</sub>Fe<sub>2</sub>As<sub>2</sub> in the B<sub>2g</sub> channel at 13 K. (b) Difference between the Raman spectra at 6 K in the SC state and in the normal state, recorded in the B<sub>2g</sub> channel for different dopings. (c) Summary of the SC pair breaking peaks and in-gap mode in Ba<sub>1-x</sub>K<sub>x</sub>Fe<sub>2</sub>As<sub>2</sub> obtained in the B<sub>2g</sub> channel. The full and open symbols correspond to results from this work and from ARPES [39, 42, 43], respectively.

tor [13]. In principle, Raman scattering with visible light is restricted to the observation of collective excitations in the singlet channel with a total momentum transfer  $\mathbf{q} = 0$ , and thus the neutron resonance mode cannot be probed directly by Raman scattering. At this point we note that the sum  $\Delta_\beta + \Delta_\alpha$  obtained from Raman data is nearly the same energy (slightly larger) as the collective mode energy, as if  $E_{CM}$  was related to an inter-band scattering process ( $\mathbf{q} \neq 0$ ). One speculative explanation lies in the observation of in-gap impurity states by ARPES below  $T_c$  [55]: light breaks a Cooper pair with a large gap out of the condensate and creates a quasi-particle on the same band with an energy cost  $\Delta_\alpha$ , while

the second particle from the broken pair is scattered into a quasi-particle state of the band with the smaller gap (energy cost  $\Delta_\beta$ ), with the help of an impurity taking the recoil for conservation of the quasi-momentum. Due to the residual interaction coming from both pairing and Coulomb interaction between two quasi-particles on different bands, and to some charge transfer between bands, the cost of this process is slightly smaller than  $\Delta_\alpha + \Delta_\beta$ . However, it is not clear within this scenario why the related Raman mode is so sharp and symmetric.

Another explanation for the  $E_{CM}$  mode is the BS exciton mechanism [19]. A recent Raman work [17] on optimally-doped Ba<sub>1-x</sub>K<sub>x</sub>Fe<sub>2</sub>As<sub>2</sub> proposed that a BS exciton mode lies between  $2\Delta_\alpha$  and  $2\Delta_\beta$  in the particle-particle channel. Within the BS scenario, all bands can strongly couple to the exciton mode, and thus the collective mode is expected to be overdamped [26, 56]. However, the mode observed in experiments is sharp, with a full-width-at-half-maximum of 10 cm<sup>-1</sup> in the OPD#2 sample and 14 cm<sup>-1</sup> in the OD sample, suggesting that the mode is decoupled from the electronic continuum and that the BS mode scenario does not capture the expected relaxational behavior.

Alternatively, the  $E_{CM}$  mode could correspond to an in-gap particle-hole exciton in the B<sub>2g</sub> channel, as predicted for a multi-band superconductor [28]. Experimentally, resonance modes in the XY geometry were observed in NaFe<sub>1-x</sub>Co<sub>x</sub>As and interpreted as particle-hole excitons originating from charge quadrupole fluctuations [26]. Indeed, local charge quadrupoles can form following partial charge transfer between non-degenerate  $d_{xz}$  and  $d_{yz}$  orbitals [26, 32]. Above  $T_S$ , charge quadrupole fluctuations dominate the response in the XY (B<sub>2g</sub>) channel and manifest themselves as a quasi-elastic peak in the low-frequency Raman spectra that is quickly suppressed below  $T_S$  [33]. However, with the structural transition suppressed near optimal doping, charge quadrupole fluctuations can grow stronger below  $T_c$ , where low-lying excitations are gapped and thus the damping of the quadrupole fluctuations is removed. In this case quadrupole fluctuations can gain coherence and lead to a particle-hole exciton mode manifesting itself as a sharp resonance in the B<sub>2g</sub> channel [25, 26]. Interestingly, the collective mode that we observe in the tetragonal phase of the optimally-doped and over-doped samples is sharper and stronger than that in the orthorhombic phase of the under-doped regime, likely due to suppressed nematic fluctuations in the orthorhombic phase, where the four-fold symmetry is broken.

## V. SUMMARY

In summary, we used electronic Raman scattering to probe the electronic properties of Ba<sub>1-x</sub>K<sub>x</sub>Fe<sub>2</sub>As<sub>2</sub> from under-doping to over-doping. We observed a quasi-elastic peak in the normal state in the B<sub>1g</sub> and B<sub>2g</sub> channels that is associated to nematic fluctuations. Upon entering the

SC state, we identified SC pair breaking peaks at energies consistent with other probes. Moreover, we observed a Raman collective mode in the  $B_{2g}$  channel with an energy similar to the neutron resonance mode. Although the nature of this Raman mode remains unclear due to the difference in the momentum transfer associated to the Raman and neutron modes, we were able to determine its evolution with doping. Interestingly, we found a phase transition or a crossover temperature in the under-doped regime below which the spectral background changes and the Raman collective mode is no longer seen, thus putting constraints on theoretical models for its origin.

## ACKNOWLEDGMENTS

We acknowledge useful discussions with K. Haule, V. K. Thorsmølle, W.-L. Zhang, P. Zhang, H. Miao, and J.-X. Yin. We acknowledge H.-H. Kung and B. Dennis with help in the experiments. This work was supported by grants from MOST (2015CB921301) and NSFC (11274362) of China. G.B. acknowledges support from the NSF Grant No. DMR-1104884 for spectroscopic characterization of pnictide materials. S.-F.W. and G.B. acknowledge support from the US Department of Energy, Basic Energy Sciences, and Division of Materials Sciences and Engineering under Grant No. de-sc0005463 for the data acquisition and analysis. H.-H. Wen acknowledges grants from MOST(2011CBA00102) and NSFC(11534005) of China.

- 
- [1] I. I. Mazin and J. Schmalian, *Physica C* **469**, 614 (2009).
- [2] S. Graser, T. A. Maier, P. J. Hirschfeld and D. J. Scalapino, *N. J. Phys.* **11**, 025016 (2009).
- [3] R. M. Fernandes and A. V. Chubukov, arXiv:1607.00865 (2016).
- [4] J. Rossat-Mignod, L. P. Regnault, C. Vettier, P. Bourges, P. Burllet, J. Bossy, J. Y. Henry, G. Lapertot, *Physica C* **185**, 86 (1991).
- [5] H. A. Mook, M. Yethiraj, G. Aeppli, T. E. Mason and T. Armstrong, *Phys. Rev. Lett.* **70**, 3490 (1993).
- [6] H. F. Fong, P. Bourges, Y. Sidis, L. P. Regnault, A. Ivanov, G. D. Gu, N. Koshizuka and B. Keimer, *Nature* **398**, 588 (1999).
- [7] Pengcheng Dai, H. A. Mook, G. Aeppli, S. M. Hayden and F. Doğan, *Nature* **406**, 965 (2000).
- [8] H. He, P. Bourges, Y. Sidis, C. Ulrich, L. P. Regnault, S. Pailhès, N. S. Berzigiarova, N. N. Kolesnikov, B. Keimer, *Science* **295**, 1045 (2002).
- [9] M. Eschrig, *Adv. Phys.* **55**, 47 (2006).
- [10] Jun Zhao, Pengcheng Dai, Shiliang Li, Paul G. Freeman, Y. Onose and Y. Tokura, *Phys. Rev. Lett.* **99**, 017001 (2007).
- [11] A. Christianson, E. Goremychkin, R. Osborn, S. Rosenkranz, M. Lumsden, C. Malliakas, I. Todorov, H. Claus, D. Chung, M. Kanatzidis, *et al.*, *Nature* **456**, 930 (2008).
- [12] C. Zhang, M. Wang, H. Luo, M. Wang, M. Liu, J. Zhao, D. L. Abernathy, T. A. Maier, K. Marty, M. D. Lumsden, S. Chi, S. Chang, J. A. Rodriguez-Rivera, J. W. Lynn, T. Xiang, J. Hu, and P. Dai, *Sci. Rep.* **1**, 115 (2011).
- [13] P. Richard, T. Sato, K. Nakayama, S. Souma, T. Takahashi, Y.-M. Xu, G. F. Chen, J. L. Luo, N. L. Wang, and H. Ding, *Phys. Rev. Lett.* **102**, 047003 (2009).
- [14] L. Shan, J. Gong, Y.-L. Wang, B. Shen, X. Hou, C. Ren, C. Li, H. Yang, H.-H. Wen, S. Li, and P. Dai, *Phys. Rev. Lett.* **108**, 227002 (2012).
- [15] R. Fernandes, A. Chubukov, and J. Schmalian, *Nature physics* **10**, 97 (2014).
- [16] F. Kretzschmar, B. Muschler, T. Böhm, A. Baum, R. Hackl, H.-H. Wen, V. Tsurkan, J. Deisenhofer, and A. Loidl, *Phys. Rev. Lett.* **110**, 187002 (2013).
- [17] T. Böhm, A. F. Kemper, B. Moritz, F. Kretzschmar, B. Muschler, H.-M. Eiter, R. Hackl, T. P. Devereaux, D. J. Scalapino, and H.-H. Wen, *Phys. Rev. X* **4**, 041046 (2014).
- [18] T. Böhm, R. Hosseinian Ahangharnejhad, D. Jost, A. Baum, B. Muschler, F. Kretzschmar, P. Adelman, T. Wolf, Hai-Hu Wen, J.-H. Chu, I. R. Fisher and R. Hackl, arXiv:1608.02772 (2016).
- [19] A. Bardasis and J. R. Schrieffer, *Phys. Rev.* **121**, 1050 (1961).
- [20] T. Tsuneto, *Phys. Rev.* **118**, 1029 (1960).
- [21] M. V. Klein and S. B. Dierker, *Phys. Rev. B* **29**, 4976 (1984).
- [22] M. V. Klein, *Phys. Rev. B* **82**, 014507 (2010).
- [23] W.-C. Lee, S.-C. Zhang, and C. Wu, *Phys. Rev. Lett.* **102**, 217002 (2009).
- [24] D. J. Scalapino and T. P. Devereaux, *Phys. Rev. B* **80**, 140512 (2009).
- [25] Y. Gallais, I. Paul, L. Chauviere, and J. Schmalian, *Phys. Rev. Lett.* **116**, 017001 (2016).
- [26] V. K. Thorsmølle, M. Khodas, Z. P. Yin, C. Zhang, S. V. Carr, P. Dai, and G. Blumberg, *Phys. Rev. B* **93**, 054515 (2016).
- [27] A. V. Chubukov, I. Eremin, and M. M. Korshunov, *Phys. Rev. B* **79**, 220501 (2009).
- [28] M. Khodas, A. V. Chubukov, and G. Blumberg, *Phys. Rev. B* **89**, 245134 (2014).
- [29] B. Shen, H. Yang, Z.-S. Wang, F. Han, B. Zeng, L. Shan, C. Ren, and H.-H. Wen, *Phys. Rev. B* **84**, 184512 (2011).
- [30] T. P. Devereaux and R. Hackl, *Rev. Mod. Phys.* **79**, 175 (2007).
- [31] M. Rahlénbeck, G. L. Sun, D. L. Sun, C. T. Lin, B. Keimer, and C. Ulrich, *Phys. Rev. B* **80**, 064509 (2009).
- [32] W.-L. Zhang, P. Richard, H. Ding, A. S. Sefat, J. Gillett, S. E. Sebastian, M. Khodas, and G. Blumberg, arXiv:1410.6452 (2014).
- [33] Y. Gallais, R. M. Fernandes, I. Paul, L. Chauvière, Y.-X. Yang, M.-A. Méasson, M. Cazayous, A. Sacuto, D. Colson, and A. Forget, *Phys. Rev. Lett.* **111**, 267001 (2013).
- [34] F. Kretzschmar, T. Böhm, U. Karahasanovic, B. Muschler, A. Baum, D. Jost, J. Schmalian, S. Caprara,

- M. Grilli, C. Di Castro, J. G. Analytis, J.-H. Chu, I. R. Fisher, and R. Hackl, *Nature Phys.* **12**, 560 (2016).
- [35] T. Böhm, R. Hosseinian Ahangharnejhad, D. Jost, A. Baum, B. Muschler, F. Kretzschmar, P. Adelman, T. Wolf, H.-H. Wen, J.-H. Chu, *et al.*, *physica status solidi (b)* (2016).
- [36] J. J. Ying, X. F. Wang, T. Wu, Z. J. Xiang, R. H. Liu, Y. J. Yan, A. F. Wang, M. Zhang, G. J. Ye, P. Cheng, J. P. Hu, and X. H. Chen, *Phys. Rev. Lett.* **107**, 067001 (2011).
- [37] E. Blomberg, M. Tanatar, R. Fernandes, I. Mazin, B. Shen, H.-H. Wen, M. Johannes, J. Schmalian, and R. Prozorov, *Nat. Commun.* **4**, 1914 (2013).
- [38] S.-F. Wu, W.-L. Zhang, D. Hu, H.-H. Kung, A. Lee, H.-C. Mao, P.-C. Dai, H. Ding, P. Richard, and G. Blumberg, arXiv:1607.06575 (2016).
- [39] Y.-M. Xu, P. Richard, K. Nakayama, T. Kawahara, Y. Sekiba, T. Qian, M. Neupane, S. Souma, T. Sato, T. Takahashi, *et al.*, *Nat. Commun.* **2**, 394 (2011).
- [40] G. Jing, H. Xing-Yuan, Z. Jun, J. Yun-Yin, G. Ya-Dong, S. Bing, R. Cong, L. Chun-Hong, and S. Lei, *Chin. Phys. B* **24**, 077402 (2015).
- [41] J.-P. Castellan, S. Rosenkranz, E. A. Goremychkin, D. Y. Chung, I. S. Todorov, M. G. Kanatzidis, I. Eremin, J. Knolle, A. V. Chubukov, S. Maiti, M. R. Norman, F. Weber, H. Claus, T. Guidi, R. I. Bewley, and R. Osborn, *Phys. Rev. Lett.* **107**, 177003 (2011).
- [42] H. Ding, P. Richard, K. Nakayama, K. Sugawara, T. Arakane, Y. Sekiba, A. Takayama, S. Souma, T. Sato, T. Takahashi, *et al.*, *Europhys. Lett.* **83**, 47001 (2008).
- [43] L. Zhao, H.-Y. Liu, W.-T. Zhang, J.-Q. Meng, X.-W. Jia, G.-D. Liu, X.-Li Dong, G.-F. Chen, J.-L. Luo, N.-L. Wang, W. Lu, G.-L. Wang, Y. Zhou, Y. Zhu, X.-Y. Wang, Z.-Y. Xu, C.-T. Chen and X.-J. Zhou, *Chin. Phys. Lett.* **25**, 4402 (2008).
- [44] K. Nakayama, T. Sato, P. Richard, Y.-M. Xu, Y. Sekiba, S. Souma, G. Chen, J. Luo, N. Wang, H. Ding, *et al.*, *Europhys. Lett.* **85**, 67002 (2009).
- [45] J.-X. Yin, A. Li, X.-X. Wu, J. Li, Z. Wu, J.-H. Wang, C.-S. Ting, P.-H. Hor, X. Liang, C. Zhang, P. C. Dai, X. C. Wang, C. Q. Jin, G. F. Chen, J. P. Hu, Z. Q. Wang, and S. H. Pan, arXiv:1602.04949 (2016).
- [46] K. Nakayama, T. Sato, P. Richard, Y.-M. Xu, T. Kawahara, K. Umezawa, T. Qian, M. Neupane, G. F. Chen, H. Ding, and T. Takahashi, *Phys. Rev. B* **83**, 020501(R) (2011).
- [47] C. Lee, K. Kihou, J. Park, K. Horigane, K. Fujita, F. Waßer, N. Qureshi, Y. Sidis, J. Akimitsu, and M. Braden, *Sci. Rep.* **6** (2016).
- [48] Y. Xu, Y. Huang, X. Cui, E. Razzoli, M. Radovic, M. Shi, G. Chen, P. Zheng, N. Wang, C. Zhang, *et al.*, *Nature Phys.* **7**, 198 (2011).
- [49] G. Li, W. Z. Hu, J. Dong, Z. Li, P. Zheng, G. F. Chen, J. L. Luo, and N. L. Wang, *Phys. Rev. Lett.* **101**, 107004 (2008).
- [50] X. G. Luo, M. A. Tanatar, J.-Ph. Reid, H. Shakeripour, N. Doiron-Leyraud, N. Ni, S. L. Bud'ko, P. C. Canfield, H. Luo, Z. Wang, H.-H. Wen, R. Prozorov and L. Taillefer, *Phys. Rev. B* **80**, 140503(R) (2009).
- [51] A. Böhrmer, F. Hardy, L. Wang, T. Wolf, P. Schweiss, and C. Meingast, *Nat. Commun.* **6** (2015).
- [52] J. M. Allred, S. Avci, D. Y. Chung, H. Claus, D. D. Khalyavin, P. Manuel, K. M. Taddei, M. G. Kanatzidis, S. Rosenkranz, R. Osborn, and O. Chmaissem, *Phys. Rev. B* **92**, 094515 (2015).
- [53] D. D. Khalyavin, S. W. Lovesey, P. Manuel, F. Krüger, S. Rosenkranz, J. M. Allred, O. Chmaissem and R. Osborn, *Phys. Rev. B* **90**, 174511 (2014).
- [54] L. Wang, F. Hardy, A. E. Böhrmer, T. Wolf, P. Schweiss and C. Meingast, *Phys. Rev. B* **93**, 014514 (2016).
- [55] P. Zhang, P. Richard, T. Qian, X. Shi, J. Ma, L.-K. Zeng, X.-P. Wang, E. Rienks, C.-L. Zhang, P. Dai, Y.-Z. You, Z.-Y. Weng, X.-X. Wu, J. P. Hu, and H. Ding, *Phys. Rev. X* **4**, 031001 (2014).
- [56] S. Maiti and P. J. Hirschfeld, *Phys. Rev. B* **92**, 094506 (2015).